

# Heat Accumulation Effects during Ultrashort Pulse Laser Ablation with Spatially Shaped Beams

Dmitriy Mikhaylov<sup>1,3</sup>, Thomas Kiedrowski<sup>2</sup>, and Andrés Fabián Lasagni<sup>3,4</sup>

<sup>1</sup> Robert Bosch Manufacturing Solutions GmbH, Wernerstr. 51, 70469 Stuttgart, Germany  
E-mail: dmitriy.mikhaylov@de.bosch.com

<sup>2</sup> Robert Bosch GmbH, Robert-Bosch-Campus 1, 71272 Renningen, Germany

<sup>3</sup> Institut für Fertigungstechnik, Technische Universität Dresden, Zeunerbau, George-Bähr-Str. 3c, 01069 Dresden, Germany

<sup>4</sup> Fraunhofer-Institut für Werkstoff- und Strahltechnik IWS, Winterbergstr. 28, 01277 Dresden, Germany

Ultrashort pulse (USP) lasers are widely used for milling, drilling and cutting applications. Their main advantages are the ability to process a broad range of different materials as well as allowing high precision ablation and yield of low surface roughness. However, until now relatively low volumetric ablation rates are obtainable for the USP milling processes. In the present study, we concentrate on the prediction of the shortest processing time required to ablate a specific geometry in a specific body. For that we discuss possibilities to increase the ablation rate for the application of laser milling of metals. Pulse energy, repetition rate and focal beam size are defined as free parameters of the ablation process thus controlling the ablation rate. The heat accumulation effect in the bulk material and reaching of a critical, material specific surface temperature are assumed to be the limiting factors for the indefinite increase of the ablation rate. An analytical model for heat accumulation during USP laser ablation of geometrically limited bodies is extended to be applied to the process with spatially shaped beams. The thermal limit of the ablation rate is determined by means of the developed model. In order to further develop the process strategy of laser beam stamping, demand for new beam shaping systems and laser sources with high pulse energies is derived from the simulation results.

DOI: 10.2961/jlmn.2018.02.0008

**Keywords:** ultrashort pulse lasers, ablation rate, milling, heat accumulation, critical temperature, laser beam stamping, beam shaping, spatial light modulator

## 1. Introduction

Application of ultrashort pulse (USP) lasers for drilling, cutting, marking and milling processes have become state of the art not only in the research environment but also in the manufacturing industry. The availability of industrial USP laser sources and precise positioning systems makes it possible to deploy this technology in 24/7-production lines [1]. Since their invention USP laser systems experience an ongoing increase of pulse energy, repetition rate and beam quality characteristics. Furthermore, optical guiding and steering systems, e.g. scanners became more precise, additionally the scanning speed increased, which not only allows to optimize the already established processes but also to use the USP technology in new application fields.

For the purpose of milling bulk materials, USP laser technology mainly competes with mechanical micro-milling, electroetching and ion beam technology. When choosing, which manufacturing technology will be deployed for series production, the technology's productivity is a highly important factor for decision making. For milling applications, productivity is represented by the ablation rate, describing how much bulk volume is removed per unit of time. The ablation rate of USP laser processes can in some extent be increased by scaling up of average laser power i.e., increasing the pulse energy, repetition rate or both [2]. Furthermore, the

wavelength, pulse duration and the burst mode affect the ablation rate as well [3]-[5]. However, the ablation rate highly depends on the specific geometry that will be ablated from a specific body.

Among limiting effects for the enhancement of ablation rate, the heat accumulation is probably the most important one. It is well known that the USP laser ablation is not a "cold" process as it was promoted when the process was introduced. A significant part of the laser power that is absorbed by the bulk material is delivered as heat [6]. This heat accumulates with each laser pulse and leads to a temperature rise of the processed part and hence its surface. For the scanning ablation of metals, Bauer et al. [7] reported some critical scanning velocity underneath which the ablated surface becomes dark and bumpy. The ablated surface stays smooth and shiny only if a scanning velocity above a critical value is used. The critical velocity is correlated with a threshold temperature, which leads to the reduction of the ablation quality when it is exceeded. The authors develop a heat accumulation model and predict the threshold temperature to be  $T_{th} = 607$  °C for stainless steel 1.4301, pulse duration  $\tau_p = 6$  ps and wavelength  $\lambda = 1030$  nm.

In our work, we aim to determine which is the shortest time required to ablate a given structure geometry from a given geometrically bounded body. As example, a real part

will be manufactured by USP laser and discussed. A 3D image of the so called swirl plate is shown in Fig. 1. The bulk volume to be ablated is approx.  $0.2 \text{ mm}^3$  and makes up only 2% of the total body volume. The ablation depth of  $100 \mu\text{m}$  however accounts for 50% of the whole thickness of the plate, which makes the swirl plate an interesting case study. The high ratio between the ablation depth and the body thickness as well as the small bulk volume underneath the ablation geometry leads to high heat accumulation in the swirl plate during the ablation process. The surface to be treated for this part is approximately  $2 \text{ mm}^2$ .

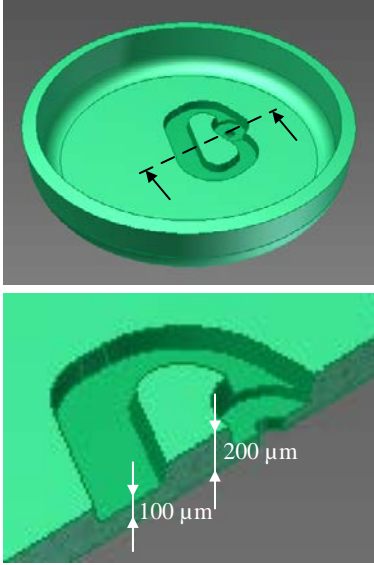


**Fig. 1** Top: 3D-View of the swirl geometry that has to be USP laser milled in the swirl plate. Bottom: Cut through the swirl plate demonstrates the ratio between the ablation depth and the plate thickness. The total diameter of the part is 5 mm.

## 2. Heat accumulation model

### 2.1 Theoretical considerations

We assume that the heat accumulation effect is the only limiting factor for scaling up of the ablation rate. For that the threshold temperature  $T_{th} = 607 \text{ }^\circ\text{C}$  as reported by [7] is assumed as a boundary condition for the process development. To determine the free process parameters, several considerations have to be done. The USP ablation rate can be expressed by:

$$\dot{V}_{abl} = f_{rep} \cdot \Delta V_p = f_{rep} \cdot \iint z_{pabl}(x, y) dx dy, \quad (1)$$

where  $\dot{V}_{abl}$  is the ablated volume per unit of time,  $f_{rep}$  is the laser repetition rate,  $\Delta V_p$  is the volume ablated per laser pulse and  $z_{pabl}$  is the ablation depth of each pulse. The ablation depth has to be integrated over the ablation surface to result in the ablation volume. Applying the logarithmic ablation model from [8]-[10] it can be obtained:

$$z_{pabl} = \delta \ln\left(\frac{F}{F_{th}}\right). \quad (2)$$

In the case of a Top-Hat beam profile, the ablation rate can be calculated as:

$$\dot{V}_{TopHat} = f_{rep} \cdot A_{TH} \cdot \delta \ln\left(\frac{E_p}{A_{TH} \cdot F_{th}}\right). \quad (3)$$

Similarly, for a Gaussian beam profile we obtain:

$$\dot{V}_{Gaussian} = f_{rep} \cdot \frac{\delta \pi w_0^2}{4} \cdot \ln^2\left(\frac{2E_p}{\pi w_0^2 F_{th}}\right), \quad (4)$$

where  $\delta$  denotes for the optical penetration depth,  $F$  is the applied fluence,  $F_{th}$  represents the threshold fluence,  $A_{TH}$  is the cross-section of the beam with the Top-Hat intensity distribution,  $w_0$  is the Gaussian beam radius at the focus position and  $E_p$  is the pulse energy. The free process parameters for enhancement of ablation rate are then the pulse repetition rate  $f_{rep}$ , the pulse energy  $E_p$  as well as the beam size and shape  $A_{TH}$  or  $w_0$  as can be seen in eqs. (3) and (4). The optical penetration depth and the threshold fluence will be considered as constant for simplification of the problem.

Then, the share of the laser power which is absorbed by the bulk material as heat  $P_{heat}$  can be expressed as:

$$P_{heat} = \alpha_{heat} \cdot E_p \cdot f_{rep}, \quad (5)$$

with  $\alpha_{heat}$  as the heat absorption coefficient. If convection and radiation are neglected, thermal conduction will transport the induced heat from the material surface into the bulk and can be expressed as:

$$\dot{Q}_{conduction} = -\kappa \cdot \oint_S \nabla T dS = -P_{heat}, \quad (6)$$

where  $\kappa$  is the thermal conductivity,  $S$  is the conduction surface and  $\nabla T$  is the three dimensional temperature gradient. Because the surface temperature as well as the temperature gradient have to be kept low, the heat conducting surface  $S$  from eq. (6) has to be maximized. For USP laser processing, the heat input into the bulk material can be assumed as instantaneous exposure by surface heat source. Hence, the conduction surface  $S$  is equal to the cross-section of the beam. Consequently,  $S$  will be maximized when the beam cross-section is also increased to its maximum. The geometrical limit for the extension of the beam cross-section is given by the ablation geometry. Following that, the laser beam has to be shaped to this form and will not be scanned over the ablation surface anymore. The ablation process strategy will be therefore changed to the so called laser beam ‘‘stamping’’ strategy. In this way, the number of free process parameters is then reduced to two, which are the pulse repetition rate  $f_{rep}$  and the pulse energy  $E_p$ .

### 2.2 Shaped beam profiles as heat sources

Analogously to [6] and [7], we start developing a model with an instantaneous single point source. The solution of the heat conduction equation for the temperature distribution in an infinite solid body is given by:

$$T(R, t) = \frac{Q}{\rho c (4\pi \alpha t)^{3/2}} \cdot e^{-\frac{R^2}{4\alpha t}}, \quad (7)$$

where  $T(R, t)$  is the temperature at the distance  $R$  from the instantaneous point source of energy at the time  $t$  after the exposure moment,  $Q$  is the heat deposited in the material,  $\rho$  is the material density,  $c$  is the specific heat capacity and  $\alpha$  is the thermal diffusivity.

To obtain a solution for a randomly shaped beam profile one can directly integrate eq. (7) over the given beam profile cross-section. However, in our work an intermediate step has been considered which provides a solution for a Gaussian multi-spot heat distribution. This step is required to simulate phase based spatial light modulator (SLM) for beam shaping.

SLMs are excellent optical elements capable of forming almost any desired Gaussian multi-spot distribution in the focal plane [13], [14]. Forming of closed Top-Hat profiles is however often accompanied by so called speckles [15] whereby the speckle-less Top-Hat forming techniques presented recently [16] show only low efficiency. Hence, our model has to represent the Gaussian multi-spot distribution of heat sources. The solution for a Gaussian single-spot as an instantaneous surface heat source is obtained by building an integral of the eq. (7) over the Gaussian beam profile with position-dependent fluence distribution instead of heat  $Q$ . The solution is given by:

$$T_{(x_c, y_c, z_c)}(x, y, z, t) = \frac{Q}{\pi \rho c \sqrt{\pi a t} (8 a t + w_0^2)} \cdot e^{-\frac{(x-x_c)^2 + (y-y_c)^2}{4 a t} \left( \frac{w_0^2}{8 a t + w_0^2} - 1 \right) - \frac{(z-z_c)^2}{4 a t}}, \quad (8)$$

whereby  $x_c, y_c, z_c$  are the center coordinates of the Gaussian beam and  $x, y, z$  are the coordinates where the temperature is calculated.

The solution for an arbitrary Gaussian multi-spot distribution is gained via superposing of the solution (8) for a single Gaussian beam:

$$T(x, y, z, t) = \sum_{i=1}^n T_{(x_{ci}, y_{ci}, z_{ci})}(x, y, z, t), \quad (9)$$

where  $n$  stands for the number of Gaussian beams in the multi-spot distribution. Eq. (9) can be used not only for the Gaussian multi-spot beam profiles but also for Top-Hat shapes. In this case, the distance between the neighboring Gaussian beams in the multi-spot distribution has to be small enough to build a flat beam profile. This is shown exemplary for a target shape in Fig. 2.

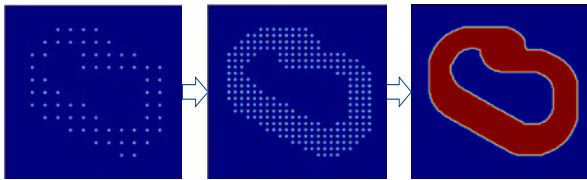


Fig. 2 Schematic representation of forming a Top-Hat profile out of superposed Gaussian beams.

### 2.3 Heat accumulation in geometrically bounded structures

Since in our example the swirl plate is a geometrically bounded body, the solutions of the heat conduction equation for an infinite body presented in eqs. (7-9) have to be further extended.

When numerical simulation, e.g. using finite difference method is applied, structures of arbitrary geometrical shapes can be modeled. However, analytical modelling solutions only exist for a limited number of shapes. To the knowledge of the authors the most complex body shape for which an analytical heat conduction solution can be found is a geometrically limited slab with parallel opposite surfaces [11].

To limit the thickness of the infinite body first to the half-infinite body and then to the infinite slab the method of fictive mirrored heat sources has been used in this study [12]. For the USP laser ablation, heat source is placed at the surface of the body. This heat source can be reflected at all ad-

iabatic body boundaries [11]. The first boundary in the  $z$  direction to be introduced is the surface where the laser pulse is applied. Because the body is limited to the top, the whole heat absorbed from the pulse will be transferred only to the bulk underneath. Hence, the heat induced by the pulse on the body surface will be doubled by the reflection at the  $xy$ -plane with  $z = 0$ . The next heat source reflection at an adiabatic body boundary takes place at the bottom of the slab as shown in Fig. 3. This new heat source might again be reflected at the upper surface, which can be also considered as an adiabatic process. The solution for the slab with restricted thickness  $H$  can hence be expressed as series expansion, whereby only a few first terms are taken into account when heat transfer is being modeled, as shown by eqs. (10) and (11):

$$T(x, y, z, t) = \sum_{s=0}^{\infty} T_{(x_c, y_c, z_{cs})}(x, y, z, t), \quad (10)$$

with

$$z_{cs} = \begin{cases} z_c + 0, & \text{for } s = 0 \\ z_c + (-1)^{s+1} \cdot 2^s \cdot H, & \text{for } s > 0 \end{cases} \quad (11)$$

and  $s$  as reflection number along the  $z$  axis.

Analogously, the introduction of fictive heat sources can be implemented by reflections in  $x$ - and  $y$ - directions [11]. By applying this method, lateral body limits will be set.

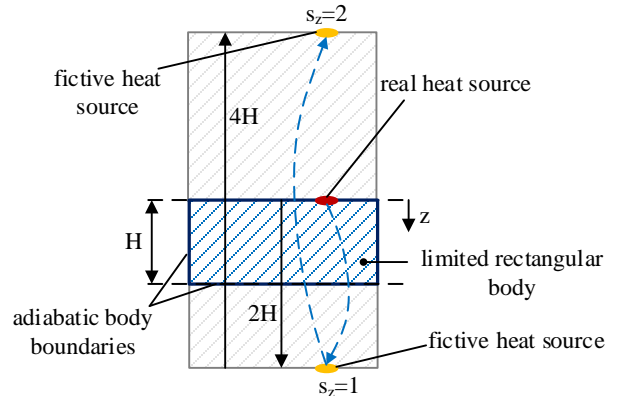


Fig. 3 Introduction of adiabatic conditions by reflection of fictive heat sources at the body boundaries.

When a shaped beam profile, consisting of multiple closely positioned Gaussian spots, is assumed, it can be mirrored in all three dimensions. In this case the number of heat sources is increased by the factor equal to the number of reflections. The solution of the heat conduction equation is then given by simple application of eq. (9) to the new amount of heat sources. The temporal development of the temperature distribution due to following pulses can be calculated by superposing the conduction equation solution of the new pulse with the temperature distribution caused by the last pulse [7].

### 2.4 Model parameters

We apply the model to calculate temperature distribution in a geometrically bounded body which is being USP laser stamped by a shaped beam profile. Material properties for the stainless steel 1.4301 displayed in Table 1 have been taken from [7]. Due to the used analytical model, the material properties were assumed to be constant with temperature.

In the heat accumulation model of the laser stamping process the Top-Hat fluence  $F$  was varied in the range between  $0.1 \text{ J/cm}^2$  and  $1.8 \text{ J/cm}^2$ . For each modeled fluence step, the number of pulses  $N_p$  required to ablate the swirl geometry with a depth  $z_{swirl} = 100 \text{ }\mu\text{m}$  was calculated by dividing  $z_{swirl}$  through  $z_{pabl}$  from eq. (2). It is clear that  $N_p$  aspires to infinity when the fluence is close to the threshold fluence and decreases with increasing fluence. By means of the model, a critical repetition rate  $f_{rep}$  was calculated for each fluence step. The critical repetition rate is defined as the highest possible laser stamping frequency which can be applied to the substrate for the time  $t_{process} = N_p/f_{rep}$  without reaching the critical surface temperature  $T_{crit}$ .

A plate thickness  $H = 0.2 \text{ mm}$  was taken into account during the simulation by application of reflected heat sources. Number of heat source reflections along the z-axis was varied between 0 and 4. The thickness itself was kept constant during the stamping simulation with analytical model. Further simulations have shown that heat source reflections along the x- or y-axes do not have any impact on the calculation results. This is the case because of the relatively large lateral dimensions of the swirl plate compared with the swirl geometry itself.

**Table 1** Material properties and model parameters used to calculate the temperature distribution during laser stamping [7]

Property	Symbol	Value	Unit
Specific heat capacity	$c$	559	J/(kg K)
Thermal diffusivity	$\alpha$	5.7	mm <sup>2</sup> /s
Density	$\rho$	7920	kg/m <sup>3</sup>
Heat absorption coefficient	$\alpha_{heat}$	0.38	[-]
Threshold fluence	$F_{th}$	0.075	J/cm <sup>2</sup>
Optical penetration depth	$\delta$	12	nm
Critical temperature	$T_{crit}$	607	°C
Initial plate temperature	$T_{init}$	23	°C

### 2.5 Simulation results and discussion

In Fig. 4, curves of the critical repetition rate are drawn over the Top-Hat fluence for  $F \in [0.2 \text{ J/cm}^2, 1.8 \text{ J/cm}^2]$ . The five different curves represent the number of heat source reflections along the z-axis used in the simulation. As it can be seen, starting from the third reflection the change of the critical repetition rate curve with increasing number of heat source reflections is marginal. However the difference between the zero z-reflections curve and the four z-reflections curve is significant. Due to the heat accumulation effects, the limited thickness of the swirl plate has to be taken into account since the body cannot be assumed half-infinite.

The critical repetition rate as well as the process duration time were also simulated for several fluences between  $0.1 \text{ J/cm}^2$  and  $1.8 \text{ J/cm}^2$ . The results are plotted in Fig. 5. The simulated data points are based on the calculation with four z-reflections of the fictive heat sources. Considering that when the fluence is zero the critical pulse repetition rate will be infinite, the plotted simulation results of the critical repetition rate can be fitted by an equation of the type  $1/x$ :

$$f_{fit} = G/F, \quad (11)$$

with  $G$  as the fitting factor, which likely depends on the body geometry as well as the heat source formation. Further investigation into the meaning of  $G$  are required. Having fitted the critical repetition rate the process duration can be forecasted for all fluences by:

$$t_{process} = \frac{z_{swirl}}{\delta \cdot \log(F/F_{th})} \cdot \frac{F}{G}. \quad (12)$$

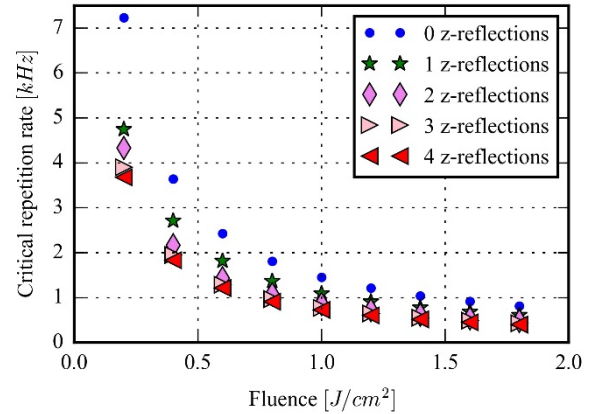


**Fig. 4** Curves of critical repetition rates over the used fluence. Depending on how many fictive source reflections were calculated, the body is either half-infinite (0 z-reflections) or limited in the thickness (>3 z-reflections).

The process duration for the swirl geometry ablation has its minimum  $t_{min} = 2.3 \text{ s}$  when fluence  $F = 0.2 \text{ J/cm}^2$  and repetition rate  $f_{rep} = 3.6 \text{ kHz}$  are used. However, the process duration curve raises rapidly when fluences lower than  $0.2 \text{ J/cm}^2$  are applied. Hence, it is advisable to use slightly higher than the optimal fluences. The process parameters and laser data for two different fluences including the optimal fluence and a fluence 2.5 times higher than the optimal are presented in Table 2.

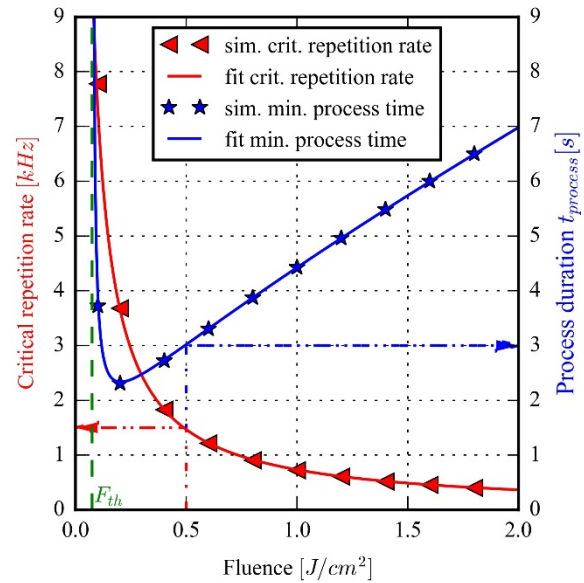


**Fig. 5** Simulation example for the swirl geometry ablation: the red curve represents the critical repetition rate over the used fluence; the blue curve denotes the process duration time for the chosen critical repetition rate.

As can be seen from Fig. 5 and from the data shown in Table 2, the average laser power, that can be utilized for swirl structure ablation is relatively low and does not rise much with higher fluences. It is much more the proportion of the pulse energy to the repetition rate that influences the process duration for the presented example. The results also indicate that for USP bulk ablation, usage of high pulse energy and low repetition rate is more beneficial rather than low pulse energy and high repetition rates. Hence, for laser stamping of geometries with ablation surfaces larger than 1 mm<sup>2</sup>, pulse energies over 1 mJ and pulse repetition rates in low kHz range show to be the most adequate parameters.

**Table 2** Laser and process parameters calculated for two laser fluences of laser stamping of the swirl geometry

	Symbol	Value		Unit
Fluence	$F$	0.2	0.5	[J/cm <sup>2</sup> ]
Repetition rate	$f_{rep}$	3.6	1.5	[kHz]
Process duration	$t_{process}$	2.3	3	[s]
Ablation rate	$\dot{V}_{abl}$	0.085	0.067	[mm <sup>3</sup> /s]
Pulse energy	$E_p$	4	10	[mJ]
Average laser power	$P_L$	14.4	15	[W]

The main advantage of the presented model is its simplicity for calculation and application. However, many physical aspects, e.g. temperature dependence of material parameters, exact body geometry, reduction of the body thickness with each pulse, were not taken into consideration. Therefore, the next step is to numerically model heat accumulation during USP laser stamping. Furthermore, if reaching of some critical temperature is not the only limiting factor for the maximization of the ablation rate, mechanical or Multiphysics modelling has to be applied, e.g. to calculate the thermal distortion of the body.

### 3. Conclusions

In the present study a method to calculate the minimum required time to ablate an arbitrary geometry in a geometrically bounded body using USP laser was developed. Heat accumulation and reaching of some specific critical temperature at the ablation surface was proclaimed to be the limiting factor for maximization of the ablation rate. Laser beam stamping was claimed to be the best way of ablating bulk volume while keeping heat accumulation low. To determine the optimal repetition rate and pulse energy for the maximum ablation rate a simple analytical model of temperature calculation for laser beam stamping process was presented. The model was based on heat conduction and a critical temperature which must not be exceeded throughout the process.

The model was applied to a chosen example geometry, being capable to determine the optimal process parameters for minimizing the processing time. The minimal process duration represents the physical limit for the USP laser ablation of the given structure for the given material, laser parameters and other boundary conditions. If different bulk material or laser are used and e.g., workpiece cooling is ap-

plied, the process duration limit will be changed. Nevertheless, the calculation results emphasize the huge potential for process time reduction down to the presented limit.

Finally, the requirements for beam guiding systems and laser sources in laser stamping application were derived: The entire potential of the USP laser stamping process can only be utilized if beam shaping optics are available which can form the laser beam profile to match the ablation structure geometry. Additionally, laser sources with high pulse energies (in the mJ-range) and low pulse repetition rate will be required.

### References

- [1] T. Kiedrowski, A. Michalowski, and F. Bauer: Laser Tech. J., 12, (2015) 30.
- [2] G. Raciukaitis, M. Brikas, P. Gecys, B. Voisiat and M. Gedvilas: J. Laser Micro/Nanoengin., 4, (2009) 186.
- [3] B. Neuenschwander, G. F. Bucher, C. Nussbaum, B. Joss, M. Mural, U. W. Hunziker and P. Schuetz: Laser Appl. in Microelectr. and Optoelectr. Manuf. XV, 7584, (2010) 75840.
- [4] B. Neuenschwander, B. Jaeggi, M. Schmid, V. Rouffing and P. E. Martin: Laser Appl. in Microelectr. and Optoelectr. Manuf. XVII, 8243, (2012) 824307.
- [5] T. Kramer, B. Neuenschwander, B. Jäggi, S. Remund, U. Hunziker and J. Zürcher: Phys. Procedia, 83, (2016) 123.
- [6] R. Weber, T. Graf, P. Berger, V. Onuseit, M. Wiedenmann, C. Freitag and A. Feuer: Opt. Express, 22, (2014) 11312.
- [7] F. Bauer, A. Michalowski, T. Kiedrowski and S. Nolte: Opt. Express, 23, (2015) 1035.
- [8] B. N. Chichkov, C. Momma, S. Nolte, F. von Alvensleben and A. Tünnermann: Appl. Phys. A, 63, (1996) 109.
- [9] C. Momma, B. N. Chichkov, S. Nolte, F. von Alvensleben, A. Tünnermann, H. Welling and B. Welleghausen: Opt. Comm., 129, (1996) 134.
- [10] C. Momma, S. Nolte, B. N. Chichkov, F. von Alvensleben and A. Tünnermann: Appl. Surf. Sci., 109, (1997) 15.
- [11] K. M. Gatovski, V.A. Karkhin: "Teoriya svarochnih deformazi i napryazheni", (Leningradski korablestroitelni institute, Leningrad, 1980) p.40. (in Russian)
- [12] D. Radaj: "Heat effects of welding temperature field, residual stress, distortion", (Springer, Berlin, Heidelberg, 1992).
- [13] Z. Kuang, D. Liu, W. Perrie, S. Edwardson, M. Sharp, E. Fearon and K. Watkins: Appl. Surf. Sci., 255, (2009) 6582.
- [14] Z. Kuang, W. Perrie, S. P. Edwardson, E. Fearon and G. Dearden: J. Phys. D: Appl. Phys., 47, (2014) 115501.
- [15] J. Strauß, T. Häfner, M. Dobler, J. Heberle and M. Schmidt: Phys. Procedia, 83, (2016) 1160.
- [16] D. Liu, Y. Wang, Z. Zhai, Z. Fang, Q. Tao, W. Perrie ... and G. Dearden: Opt. Laser Technol., 102, (2018) 68.

(Received: July 12, 2018, Accepted: September 6, 2018)